Simulating wave runup on an intermediate–reflective beach using a wave-resolving and a wave-averaged version of XBeach

de Beer, A. F.; McCall, R. T.; Long, J. W.; Tissier, M. F.S.; Reniers, A. J.H.M.

DOI
10.1016/j.coastaleng.2020.103788

Publication date
2021

Document Version
Final published version

Published in
Coastal Engineering

Coastal Engineering 163 (2021) 103788

Contents lists available at ScienceDirect

Coastal Engineering

journal homepage: http://www.elsevier.com/locate/coastaleng

Simulating wave runup on an intermediate–reflective beach using a wave-resolving and a wave-averaged version of XBeach

A.F. de Beer [a,b,1], R.T. McCall [a,*], J.W. Long [c,2], M.F.S. Tissier [b], A.J.H.M. Reniers [b]

[a] Deltares, Boussinesqweg 1, P.O. Box 177, 2600, MH Delft, the Netherlands
[b] Delft University of Technology, Faculty of Civil Engineering and Geosciences, Delft, the Netherlands
[c] St. Petersburg Coastal and Marine Science Center, US Geological Survey, St. Petersburg, Florida, USA

ARTICLE INFO

Keywords:
Swash
Runup
Infragravity waves
XBeach
Non-hydrostatic modeling

ABSTRACT

The prediction of wave runup, as well as its components, time-averaged setup and the time-varying swash, is a key element of coastal storm hazard assessments, as wave runup controls the transitions between morphodynamic response types such as dune erosion and overwash, and the potential for flooding by wave overtopping. While theoretically able to simulate the dominant low-frequency swash, previous studies using the infragravity-wave–resolving model XBeach (XBSB) have shown an underestimation of the observed swash variance and wave runup, which was in part related to the absence of incident-band swash motions in the model. Here, we use an incident-band wave-resolving, non-hydrostatic version of the XBeach model (XBNH) to simulate wave runup observed during the SandyDuck '97 experiment on an intermediate–reflective sandy beach. The results show that the XBNH model describes wave runup and the individual setup and swash components well. We subsequently examine differences in wave runup prediction between the XBSB and XBNH models and find that the XBNH model is a better predictor of wave runup than XBSB for this beach, which is due to better predictions of both the incident-band and infragravity-band swash. For a range of beach states from reflective to dissipative it is shown that incident-band swash is underestimated by XBSB relative to XBNH, in particular for reflective conditions. Infragravity-band swash is shown to be lower in XBSB than XBNH for most conditions, including dissipative conditions for which the mean difference is 16% of the deep water wave height. The difference in infragravity-band swash in XBNH relative to XBSB is shown to mainly be the result of processes occurring outside the swash zone, but approximately 15% of the difference is caused by explicitly resolving incident-band wave motions within the swash zone, such as swash-swash interactions, which inherently cannot be simulated by wave-averaged models.

1. Introduction

Following wave breaking in the surf zone, waves propagate through the swash zone in the form of a bore (Brocchini and Baldock, 2008), translating into runup on the beach. Under energetic conditions wave runup determines the potential for coastal erosion and flooding by steering the transition between morphodynamic response types (e.g., beach erosion to dune erosion, and dune erosion to overwash; Sallenger, 2000), and driving overtopping of structures (Van der Meer and Stam, 1992) and overwash of coastal dunes (Matias et al., 2016). As the population in coastal areas increases and sea levels rise (e.g., Neumann et al., 2015), the prediction of coastal storm impacts becomes ever more relevant, thereby increasing the need for accurate and efficient predictions of wave runup.

A commonly used parameterization for runup on sandy coasts was developed by Stockdon et al. (2006), hereafter called S2006, by fitting a large number of observations from a range of beaches and wave conditions to a parametric model based on deep water significant wave height (H_0), peak deep water wave length (L_0) and foreshore beach slope (β_f). It was shown by Stockdon et al. (2006) that runup is best parameterized when splitting the motion of the shoreline into two components: setup and swash. Setup ($\overline{\eta}$) is the time-averaged,

* Corresponding author.
E-mail address: Robert.McCall@deltares.nl (R.T. McCall).
[1] Currently at Royal HaskoningDHV, Rotterdam, The Netherlands.
[2] Currently at Department of Earth and Ocean Sciences, University of North Carolina Wilmington, North Carolina, USA.

https://doi.org/10.1016/j.coastaleng.2020.103788
Received 1 September 2019; Received in revised form 25 June 2020; Accepted 17 September 2020
Available online 30 September 2020

Lagrangian water level elevation at the shoreline relative to still water level (η), and is driven by cross-shore gradients in radiation stress (Longuet-Higgins and Stewart, 1964). Swash is the time-varying component of the shoreline, which can be subdivided into the significant incident-band ($f > 0.05$ Hz; S_{inc}) and infragravity-band ($f \leq 0.05$ Hz; S_{ig}) swash following:

$$S_{inc} = 4\sqrt{\int_{0.05}^{\infty} E_{\eta}(f)df} \tag{1a}$$

$$S_{ig} = 4\sqrt{\int_{0}^{0.05} E_{\eta}(f)df} \tag{1b}$$

where $E_{\eta}(f)$ is the variance density of the shoreline motion and f is frequency.

While the parameterization of Stockdon et al. (2006) performs well for both dissipative and reflective beaches under mildly-energetic conditions, the observations used to derive the relations ranged up to a maximum offshore wave height of 4 m, meaning that the parameterization may not be valid for more extreme conditions (e.g., hurricane conditions; Stockdon et al., 2014). To fill this observational gap, runup data can be generated synthetically using a validated process-based numerical model. Stockdon et al. (2014) attempted to validate the process-based numerical model XBeach (Roelvink et al., 2009) in infragravity-wave resolving mode (surf-beat mode, henceforth called XBSB) for wave runup observed during the SandyDuck '97 experiment (henceforth SD97). In the XBSB model, infragravity wave motions are fully resolved using the non-linear shallow water equations, but incident-band wave motions are parameterized using a short wave action balance that describes variations at the wave-group time scale, but not intra-wave motions on the incident-band wave time scale (see e.g., Roelvink et al., 2017). This parameterization is considered valid on dissipative beaches, where infragravity-band motions dominate the swash and the incident-band swash is saturated due to wave breaking (Guza and Thornton, 1982; Ruessink et al., 1998). On the intermediate–reflective beach of SD97, Stockdon et al. (2014) found that XBSB significantly underestimated runup, which was the result of both a large underestimation of S_{inc}, as well as an underestimation of S_{ig}. In similar studies using XBSB, the model was found to underestimate observed S_{inc} and S_{ig} in a laboratory dune erosion experiment (Palmsten and Splinter, 2016), and, to lesser extent, underestimate S_{ig} on a high-energy dissipative beach (Cohn and Ruggiero, 2016). While an underestimation of S_{inc} by XBSB may be expected due to the wave-averaged modeling approach, the underestimation of S_{ig} by XBSB suggests that the model may also be missing physical processes occurring at the infragravity time scale.

Nicolae Lerma et al. (2017) showed that wave runup on a dissipative beach (Le Truc Vert; Senechal et al., 2011) was well described by an incident-band wave-resolving, non-hydrostatic model (SWASH; Zijlema et al., 2011). The skill of the wave-resolving model was suggested to be an improvement over the earlier work of Stockdon et al. (2014), although no direct comparison between the phase-resolving model and the infragravity-wave–resolving model XBSB was carried out. These results suggest that an improvement in the predictive wave runup skill of the XBeach model may be achieved by explicitly resolving incident-band swash motions, leading to better predictions of S_{inc}, as well as potentially better predictions of S_{ig} through a better description of the nearshore wave spectrum and the explicit simulation of swash-swash interactions (e.g., Brocchini and Baldock, 2008). In this study we investigate this potential by using the XBeach non-hydrostatic model (Smit et al., 2010; McCall et al., 2014), henceforth termed XBNH, which resolves incident-band wave motions in intermediate and shallow water depths in a similar manner to the SWASH model (Zijlema et al., 2011). XBNH has previously been applied to simulate wave runup on reflective gravel beaches (McCall et al., 2014; Poate et al., 2016) and coastal structures (Roelvink et al., 2017), and on infragravity-dominated coral reef-lined coasts (Pearson et al., 2017; Lashley et al., 2018; Klaver et al., 2019), but has not previously been used to study runup on sandy coasts under a variety of dissipative and reflective wave conditions. Nor has a comprehensive analysis been made of the simulated swash dynamics in XBSB and XBNH to identify potential sources of S_{ig} underestimation in the XBSB model and the conditions under which this underestimation may occur. In this paper we first assess the ability of the XBNH model to reproduce observed incident-band and infragravity-band wave transformation, $\bar{\eta}$, S_{inc}, S_{ig} and combined runup during the SD97 field experiment. We subsequently build upon the work of Stockdon et al. (2014) by comparing results from the XBNH model with results from the XBSB model to analyse differences in predicted swash motions, identify sources that can lead to an underestimation of swash variance in XBSB, and identify potential limitations in the application of XBSB.

2. Methodology

To investigate the skill of XBNH in predicting wave runup, model outputs are compared to runup data from the SD97 field experiment. This experiment was completed at the U.S. Army Corps of Engineers Field Research Facility (FRF) in Duck, North Carolina, in October 1997 (Fig. 1). Duck is an intermediate–reflective beach with an average foreshore beach slope of 0.10 (Stockdon et al., 2006). We use runup data collected from October 16–24 for model validation and calibration, in line with Stockdon et al. (2014). A short description of the data is given, after which the XBNH model setup is discussed.

2.1. Observations

Near-daily bathymetry measurements were collected during the experiment (Fig. 2). Two-dimensional frequency-directional wave spectra were collected by an array of 15 bottom-mounted pressure sensors located in approximately 8 m water depth (FRF-8 m array). The spectra are characterized by low to intermediate wave energy conditions with a small storm occurring around October 19 and fairly shore normal angles of incidence (Fig. 3 a and c). Due to changing wave conditions during the observation period, the beach state varied between reflective and dissipative (cf. Wright and Short, 1984). Tidal water levels were measured every 6 min at a tide gauge at the seaward end of the FRF pier at approximately 8 m depth (Fig. 3 d). Hydrodynamic pressure was measured at 55 pressure gauges at depths ranging from 5.3 to 1.5 m (Fig. 2 a) at a frequency of 2 Hz and transformed to significant incident-band wave height (0.05–0.25 Hz) by Stockdon et al. (2014). Similarly, raw pressure time series were used to compute significant infragravity wave heights in the frequency band lower than 0.05 Hz for the purpose of this study.

Time series of wave runup were collected at six alongshore locations using video images collected at a frequency of 2 Hz (Stockdon et al., 2006) for 17 min every daylight hour (Fig. 2 a). Runup time series were converted to statistics of shoreline setup, and significant incident and infragravity swash using Equation (1) (Stockdon et al., 2006).

2.2. XBeach model

The Kingsday version of the XBNH model was used to model the hydrodynamic conditions during the SD97 field experiment. XBNH resolves depth-averaged flow and surface elevation variations on the timescale of individual waves using the shallow water equations extended with a non-hydrostatic pressure term. The model is able to simulate wave propagation accurately in shallow–intermediate water depths ($kh \leq 3$, where k is the wave number and h is the water depth). The model employs the hydrostatic front approximation of Smit et al. (2013) to improve the location of wave breaking and the dissipation rate in shallow water. The model continuity and momentum equations are

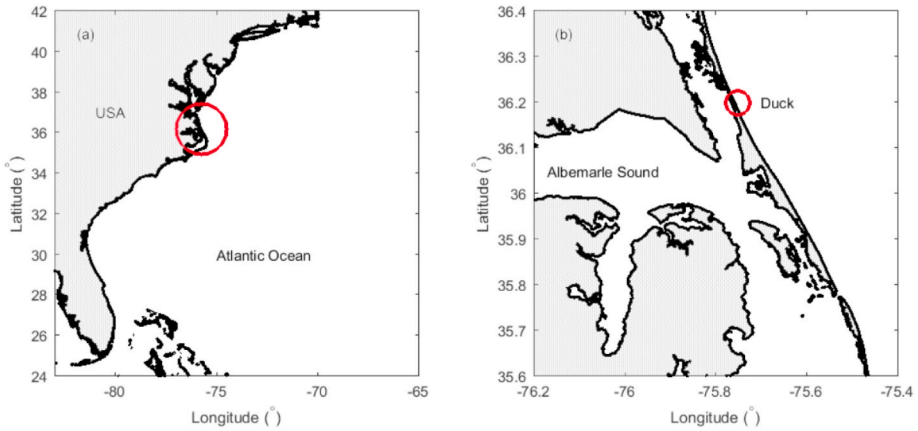

Fig. 1. Location of Duck, NC, on the east coast of the USA (a), on the seaward side of a barrier island fronting the mainland North Carolina coast (b).

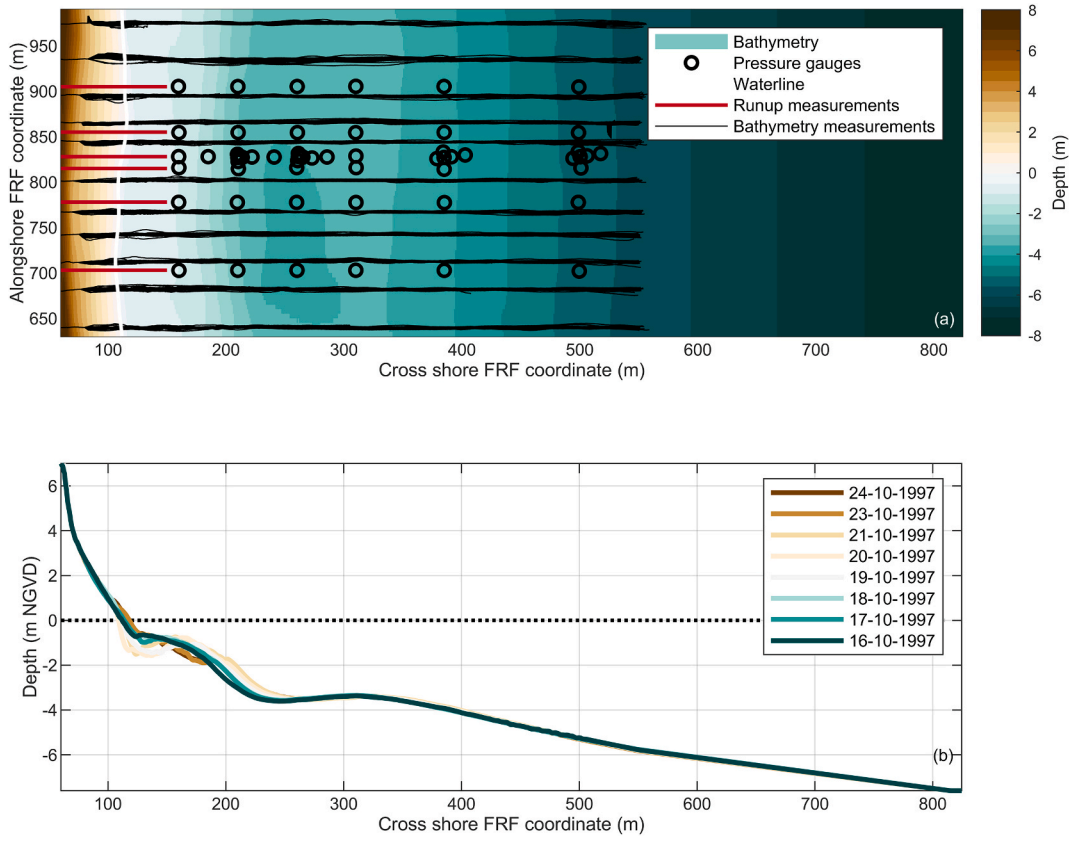

Fig. 2. Top view of the Duck, NC, XBeach domain, with relevant measuring locations; the bathymetry shown was collected on October 16 (a). The change in bathymetry along a transect at y = 830 m during the experiment (b).

given below:

$$\frac{\partial \zeta}{\partial t}+\frac{\partial hu}{\partial x}+\frac{\partial hv}{\partial y}=0 \tag{2a}$$

$$\frac{\partial u}{\partial t}+u\frac{\partial u}{\partial x}+v\frac{\partial u}{\partial y}-\nu_h\left(\frac{\partial^2 u}{\partial x^2}+\frac{\partial^2 u}{\partial y^2}\right)=-\frac{\tau_{bx}}{\rho h}-\frac{1}{\rho}\frac{\partial(\overline{q}+\rho g\zeta)}{\partial x} \tag{2b}$$

$$\frac{\partial v}{\partial t}+u\frac{\partial v}{\partial x}+v\frac{\partial v}{\partial y}-\nu_h\left(\frac{\partial^2 v}{\partial x^2}+\frac{\partial^2 v}{\partial y^2}\right)=-\frac{\tau_{by}}{\rho h}-\frac{1}{\rho}\frac{\partial(\overline{q}+\rho g\zeta)}{\delta y} \tag{2c}$$

where x and y are the horizontal spatial coordinates, t is the temporal coordinate, ζ is the Eulerian free surface elevation, u and v are the depth-averaged velocities in the cross- and alongshore direction, ν_h is the horizontal viscosity, ρ is the water density, $\overline{q}$ is the depth-averaged dynamic pressure normalized by the density, g is the gravitational constant and τ_{bx} and τ_{by} are the bed shear stresses in cross- and alongshore direction.

A 2DH model was set up with a domain size of 380 m in the alongshore and approximately 800 m in the cross-shore direction (Fig. 2). A constant grid size of 5 m was used in the alongshore direction, while the grid size in the cross-shore direction varied between 1 m at the offshore boundary and 0.2 m close to shore. The bathymetry and foreshore topography for every XBeach model run was based on the near-daily bathymetric measurements and extended to the same depth as where the wave spectra were measured at the FRF-8 m array. The frequency-

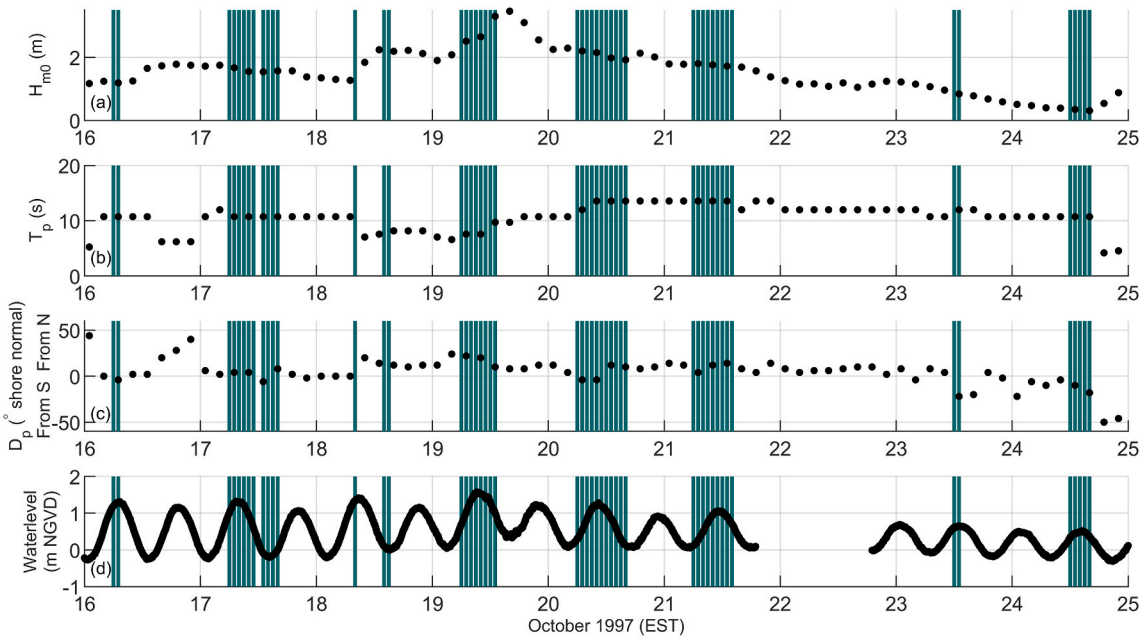

Fig. 3. Significant wave height during the experiment (a), peak period (b), the angle of wave incidence with respect to shore-normal (c) and the water level (d). For October 22 no water level data are available, therefore the data are not used. Times when runup was measured (50 instances) are indicated with green lines. Figure modified from Stockdon et al. (2014). (For interpretation of the references to colour in this figure legend, the reader is referred to the Web version of this article.)

directional spectra measured at the FRF-8 m array were used as offshore wave boundary conditions and the measured tidal water level was imposed as a uniform water level boundary condition over the entire domain. Cyclic boundary conditions were imposed on the lateral boundaries, which reduce shadow zones in the model (Roelvink et al., 2015). A total of 50 simulations, representing the same data as used by Stockdon et al. (2014), were run for a period of 22 min, constituting 5 min for model spin-up and 17 min of simulation data to correspond with the 17-min duration video-based runup observations. During each simulation a constant tidal level was assumed, as changes are minimal within a duration of 17 min. The run time for each 22-min duration simulation was approximately 45 min using a standard PC with four computational cores.

Output of waves and water levels used to compute wave runup were generated every 0.5 s and morphological changes were not included in the model simulations. Simulated significant incident-band ($H_{m0,inc}$) and infragravity-band ($H_{m0,ig}$) wave heights were computed from the zeroth-order moment of the time series of the modelled water surface elevation:

$$H_{m0,inc} = 4\sqrt{\int_{0.05}^{0.25} E_\zeta(f)df} \tag{3a}$$

$$H_{m0,ig} = 4\sqrt{\int_{0}^{0.05} E_\zeta(f)df} \tag{3b}$$

where $E_\zeta(f)$ is the variance density of the modelled Eulerian water surface elevation. Shoreline setup ($\overline{\eta}$), incident-band and infragravity-band swash (S_{inc} and S_{ig}), and the 2%-exceedence runup level ($R_{2\%}$) were computed from the time series of the simulated Lagrangian shoreline position relative to still water level (η) following Stockdon et al. (2006) and Equation (1).

Two model parameters related to bed friction and wave breaking were determined during the model calibration phase. To this end, three periods were simulated with low ($H_0 = 0.6$ m), intermediate ($H_0 = 1.7$ m) and high ($H_0 = 3.6$ m) offshore waves and model predictions of wave transformation compared to observations. Using observations of incident-band and infragravity-band wave height at the 55 pressure gauges (Fig. 2a), this calibration led to the selection of a Chezy coefficient of $C = 54\ m^{1/2}/s$ for bed friction (calibration range $C = 50$–$60\ m^{1/2}/s$) and a wave steepness criterium of 0.35 (calibration range 0.30–0.50) for the initiation of wave breaking through the hydrostatic front approximation (HFA; see Smit et al., 2013). As in other reported cases, wave transformation is relatively insensitive to the bed friction coefficient value, whereas transformation is sensitive to the parameter for the initiation of wave breaking. Calibrated settings are however in line with optimal values found in other studies using the XBNH model (e.g., Roelvink et al., 2017) and are therefore considered representative for this case-study. The water depth threshold for the definition of the waterline in the model simulations was set to 0.05 m (cf. McCall et al., 2014; Stockdon et al., 2014) to correspond with the probable water depth identified as the leading runup edge in the video images of the SD97 experiment (Stockdon et al., 2006). Note that although Stockdon et al. (2014) selected a greater value than this (0.10 m) in their study, they found that a lower value of 0.05 m led to slightly larger simulated swash amplitudes. The difference in this parameter value is accounted for in Section 4.1.

The error statistics used to define the performance of the model for predicting runup are the root mean square error (rmse), bias, the coefficient of determination (R^2) and the scatter index (SCI). With Y representing the model results and X representing the measured values, the formulations for these statistics are:

$$rmse = \sqrt{\frac{1}{n}\sum_{i=1}^{n}(Y_i - X_i)^2} \tag{4a}$$

$$bias = \frac{1}{n}\sum_{i=1}^{n}(Y_i - X_i) \tag{4b}$$

$$R^2 = \frac{\sum_{i=1}^{n}(X_i - Y_i)^2}{\sum_{i=1}^{n}\left(Y_i - \overline{X}\right)^2 + \sum_{i=1}^{n}(X_i - Y_i)^2} \tag{4c}$$

$$SCI = \frac{\sqrt{\frac{1}{n}\sum_{i=1}^{n}(Y_i - X_i)^2}}{max\left(\sqrt{\frac{1}{n}\sum_{i=1}^{n}|X_i|^2}, \overline{X}\right)} \quad (4d)$$

3. Results

3.1. Wave transformation

Wave heights in the incident and infragravity band predicted by XBNH are compared to wave heights observed at the 55 pressure gauge locations. Travelling from deeper to shallower water, observations show a shift of wave energy from the incident band to the infragravity band (see Fig. 4 for an example). Overall, this trend is well captured by the model. Quantitatively, wave heights in the incident band compare well to the observations (Fig. 5a and Table 1) with a rmse, bias and SCI of 0.17 m, −0.09 m and 0.10 respectively. Travelling from the offshore-most measurement location ($x = 500$ m) to the most nearshore location ($x = 160$ m), the rmse decreases from 0.23 m to 0.10 m while the bias shifts from −0.16 m to −0.04 m, indicating that the model performance increases towards shore. Given the lower magnitude, infragravity-band wave height is predicted slightly less well in a relative sense than incident-band wave height (Fig. 5b and Table 1), with a rmse of 0.08 m, bias of 0.01 m and SCI of 0.23. The rmse increases from 0.06 m offshore to 0.09 m near shore, and the bias from 0.00 m to 0.03 m, indicating that the model overestimation of infragravity-band wave height increases very slightly towards shore. In general, the accuracy of wave height predictions is similar to that of other model comparison studies with field data (e.g., Reniers et al., 2006; Roelvink et al., 2009; Stockdon et al., 2014; McCall et al., 2014; Rijnsdorp et al., 2015) and the model is considered sufficiently accurate at predicting surf zone wave conditions that drive runup.

3.2. Runup

XBNH runup predictions are compared to measured values of $\overline{\eta}$, S_{inc}, S_{ig} and $R_{2\%}$ (Fig. 6 and Table 2). Simulated shoreline setup corresponds reasonably well with the measurements (Fig. 6 a) with an rmse of 0.13 m and a small under prediction (bias of −0.04 m). Similar predictive skill is found for S_{inc} and S_{ig} (Fig. 6 b–c), with an rmse of 0.25 m and 0.23 m, respectively, and a bias of 0.06 m, and −0.09 m, respectively. Simulated $R_{2\%}$ also corresponds well with observations, with an rmse of 0.28 m and a bias of 0.06 m (Fig. 6 d).

In a comparative sense, the skill of the XBNH model is generally better than that of the S2006 parameterization for SD97 as found by Stockdon et al. (2014, see Table 2) for $\overline{\eta}$, S_{inc} and S_{ig} ($R_{2\%}$ not reported). Given the skill of the XBNH model in simulating swash during SD97, as well as the potential of the model to simulate more complex coastal environments, more extreme events, and morphodynamics in the future, the XBNH model may be considered a useful tool for wave runup prediction.

4. Discussion

4.1. Comparison of XBNH to XBSB

Comparisons with the SD97 data indicate that the XBNH model has better skill than the XBSB model used by Stockdon et al. (2014). To compare the XBNH model to a XBSB model that includes recent improvements to the wave groupiness prediction (Roelvink et al., 2017), a new XBSB model (Kingsday version) was set up using the same computational grid as the XBNH model. Note that this is a much finer grid than commonly used or needed for an XBSB application. Most model settings, such as the breaker parameter, were kept equal to settings used by Stockdon et al. (2014). However, changes were made to the water depth threshold for the definition of the waterline, which was set equal to that used in the XBNH simulations (0.05 m, see Section 2.2) to ensure consistency between the XBNH and XBSB models, and the wave groupiness-conserving wave transformation option (*single_dir*) was used following the recommendations of Roelvink et al. (2017). While it is not the purpose of this study to investigate differences between the 2DH XBeach model used by Stockdon et al. (2014) and the XBSB model used in this study, it may be noted that the XBSB model in this study has lower errors than those reported by Stockdon et al. (2014) for wave height (their reported rmse of 0.21–0.41 m, versus a rmse of 0.09–0.15 m for incident-band wave height and 0.09–0.12 m for infragravity-band wave height here), S_{inc} (their reported rmse of 0.82 m versus 0.63 m here) and S_{ig} (their reported rmse of 0.66 m versus 0.57 m here), and $\overline{\eta}$ (their reported rmse of 0.17 m versus 0.12 m here).

The results of the XBSB model are shown in Fig. 5 (panels c and d) and Table 1 for wave height transformation, and in Fig. 6 and Table 2 for swash hydrodynamics. Throughout much of the shoaling zone and surf zone, the incident-band wave height is predicted similarly well by XBNH and XBSB. Close to shore XBNH underestimates the incident-band wave height while XBSB overestimates the incident-band wave height (bias of −0.04 m vs. 0.05 m). The prediction of the infragravity-band wave height is different for XBNH and XBSB, with XBNH giving a slightly better prediction. XBNH very slightly overestimates wave heights (bias 0.01 m) and XBSB underestimates them to a slightly larger degree (bias −0.09 m).

Setup at the waterline is predicted similarly by the two models. The XBNH results show slightly more scatter, represented in a higher SCI and greater bias. The performance of XBNH is however much better for incident- and infragravity-band swash predictions. The rmse of XBNH

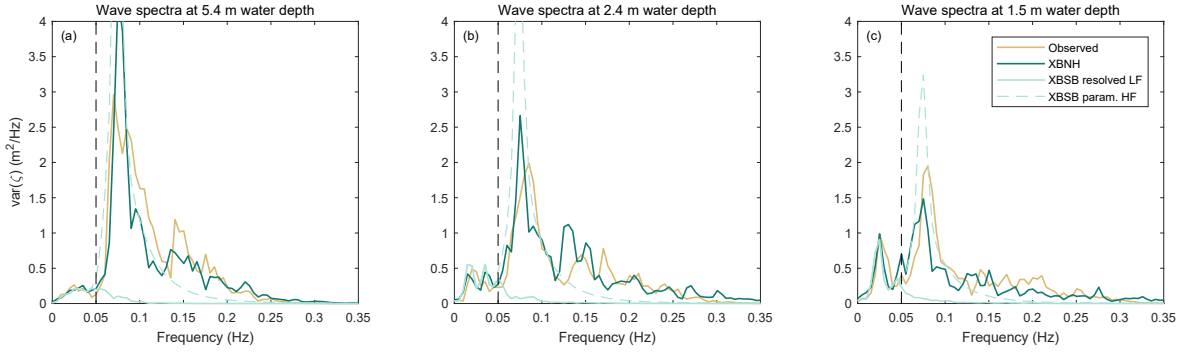

Fig. 4. Example of observed and modelled wave spectra at three water depths in a cross-shore transect, with offshore conditions of $H_{m0} = 1.57$ m and $T_p = 10.7$ s. Note that for XBSB, the low-frequency (infragravity-band; solid line) component of the spectrum is explicitly derived from the modelled water surface elevation, whereas the high-frequency (incident-band; dashed line) component is estimated using the modelled local wave height, the offshore peak period and a JONSWAP spectral shape parameterization. The frequency divide between incident band and infragravity band used in this study is marked by the vertical dashed line.

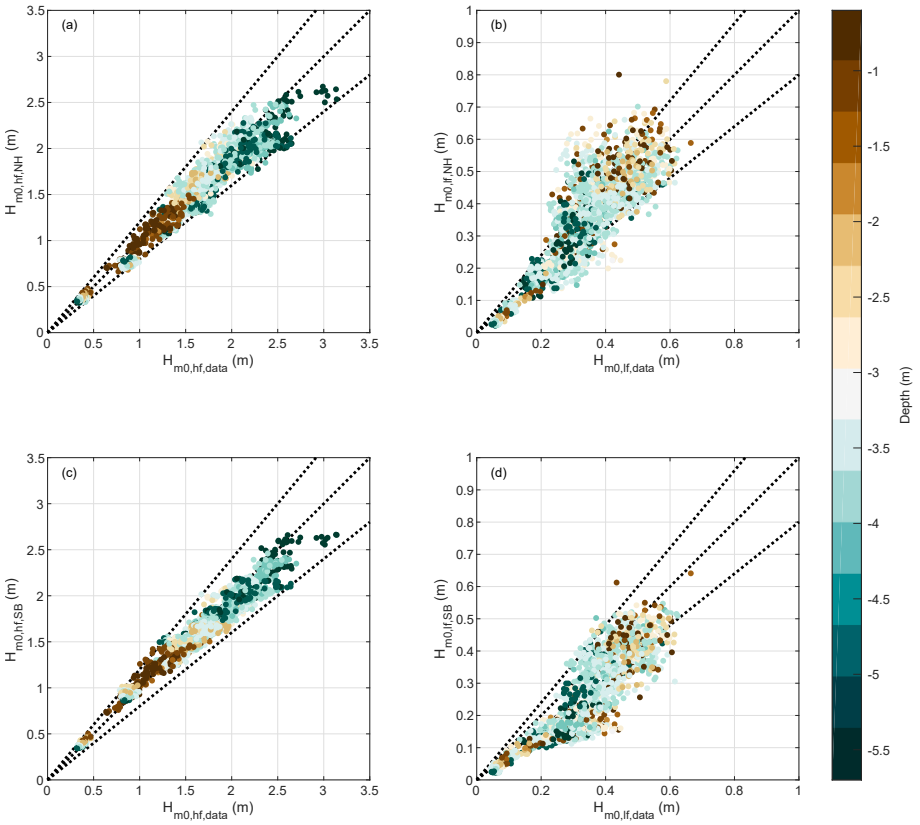

Fig. 5. Comparison of modelled and observed significant incident-band wave height (a) and significant infragravity-band wave height (b) for XBNH. Results of XBSB (see section 4) are shown in (c) and (d). Dashed lines indicate the 1:1 and 20% error lines. The color scale indicates the water depth at the observation locations. (For interpretation of the references to colour in this figure legend, the reader is referred to the Web version of this article.)

Table 1
Statistics describing the fit between observations and model results for wave height. The root mean square error (rmse), bias and scatter index (SCI) are listed for $H_{m0,inc}$ and $H_{m0,ig}$ for all 55 measuring locations together and at different locations in the cross shore. Results are shown for the XBNH model and the XBSB model (see section 4).

			Overall	x (m)					
				160	210	260	310	385	500
$H_{m0,inc}$	rmse(m)	XBNH	0.17	0.10	0.14	0.13	0.15	0.20	0.23
		XBSB	0.12	0.09	0.12	0.11	0.12	0.14	0.15
	bias(m)	XBNH	−0.09	−0.04	−0.05	−0.04	−0.08	−0.15	−0.16
		XBSB	−0.05	0.05	−0.04	−0.06	−0.07	−0.09	−0.06
	SCI(−)	XBNH	0.10	0.09	0.08	0.08	0.09	0.11	0.12
		XBSB	0.07	0.08	0.07	0.07	0.07	0.08	0.08
$H_{m0,ig}$	rmse(m)	XBNH	0.08	0.09	0.09	0.08	0.07	0.07	0.06
		XBSB	0.11	0.12	0.12	0.10	0.12	0.11	0.09
	bias(m)	XBNH	0.01	0.03	0.02	0.02	−0.01	−0.01	0.00
		XBSB	−0.09	−0.10	−0.10	−0.08	−0.09	−0.09	−0.07
	SCI(−)	XBNH	0.23	0.24	0.24	0.23	0.21	0.19	0.21
		XBSB	0.31	0.33	0.31	0.30	0.33	0.32	0.32

for incident-band swash is less than half that of XBSB, with a substantially lower absolute bias. It should be noted here that S_{inc} is computed following Equation (1) and therefore contains all swash variance at frequencies greater than 0.05 Hz, not just swash motions caused directly by individual incident-band waves. XBSB does not model short-wave motions, but because it is capable of representing infragravity wave steepening and infragravity-wave–wave group interactions, some variance is present at the waterline in the XBSB model at frequencies greater than 0.05 Hz (split frequency), but lower than the peak frequency (f_p = 0.07–0.24 Hz), resulting in a non-zero value of S_{inc} (see Fig. 7 for an example). The rmse of XBNH for infragravity-band swash is also less than half of that of XBSB and the magnitude of the bias in XBNH is much smaller than that of XBSB. Finally, $R_{2\%}$ is better predicted by XBNH, with a rmse of 0.28 m versus 0.49 m for XBSB, and a smaller bias (0.06 m overestimation in XBNH versus 0.41 m underestimation in XBSB).

Variations of the swash components in the XBNH and XBSB models relative to the dominant environmental parameters during SD97 (wave height, length, and beach slope) are analyzed and compared to those found by Stockdon et al. (2006) for a range of dissipative to reflective beaches. The S2006 relations for setup, and incident- and infragravity-band swash relative to these parameters are as follows:

$$\overline{\eta} = 0.35\beta_f \sqrt{H_0 L_0} \tag{5a}$$

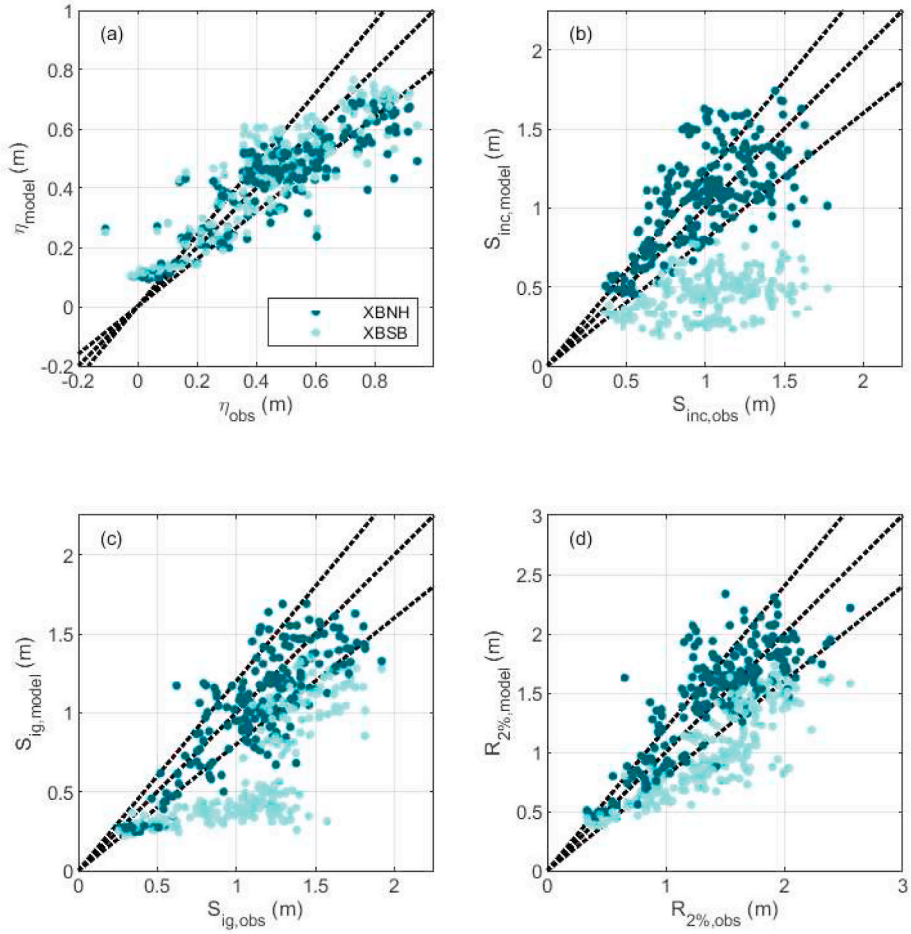

Fig. 6. Observed and modelled $\overline{\eta}$ (a), S_{inc} (b), S_{ig} (c) and $R_{2\%}$ (d) for the XBNH model (dark green). Results for the XBSB model (light green; see section 4) are shown for reference. Dashed lines indicate the 1:1 and 20% error lines. (For interpretation of the references to colour in this figure legend, the reader is referred to the Web version of this article.)

Table 2
Statistics describing the fit between observations and model results for runup. The root mean square error (rmse), bias, the coefficient of determination (R^2) and scatter index (SCI) are listed for $\overline{\eta}$, S_{inc}, S_{ig} and $R_{2\%}$ for the XBNH model and the XBSB model (see section 4). * Statistics for S2006 are included as reported by Stockdon et al. (2014), but are not available for $R_{2\%}$ and the SCI.

	Model	rmse (m)	bias (m)	R^2 (−)	SCI (−)
$\overline{\eta}$	XBNH	0.13	−0.04	0.60	0.25
	XBSB	0.12	−0.01	0.70	0.22
	S2006*	0.21	0.10	0.41	–
S_{inc}	XBNH	0.25	0.06	0.60	0.24
	XBSB	0.63	−0.56	0.45	0.59
	S2006*	0.36	0.19	0.41	–
S_{ig}	XBNH	0.23	−0.09	0.74	0.19
	XBSB	0.57	−0.51	0.53	0.48
	S2006*	0.26	−0.06	0.54	–
$R_{2\%}$	XBNH	0.28	0.06	0.73	0.19
	XBSB	0.49	−0.41	0.56	0.33
	S2006*	–	–	–	–

$$S_{inc} = 0.75\beta_f \sqrt{H_0 L_0} \tag{5b}$$

$$S_{ig} = 0.06\sqrt{H_0 L_0} \tag{5c}$$

where β_f is defined as the average beach slope over a distance of $\pm 2\sigma$ around the setup line $\overline{\eta}$, with σ the standard deviation of the water level time series at the shoreline (Stockdon et al., 2006).

Fig. 8 and Table 3 show that the lines of linear regression of the XBNH results with respect to wave height, wave length and beach slope generally correspond well with the data analyzed by Stockdon et al. (2006). While it has already been shown that the XBNH model can reasonably well simulate swash during SD97 (Table 2), these results indicate that the individual components of runup in the XBNH model vary with changing physical forcing conditions in a similar way to those found by Stockdon et al. (2006) for a large range of beaches. While further validation is required, this behaviour suggests that the underlying physics are well described and that the XBNH model may provide similar predictive skill on other beaches. For XBSB however, a significantly lower slope of linear regression is found for the incident-band swash (0.28, which is only 37% of the slope of S2006; see Table 3) and the infragravity-band swash (0.04, which is 67% of the slope of S2006). The infragravity-band swash in XBSB is particularly underestimated relative to S2006 and XBNH for moderately energetic conditions ($\sqrt{H_0 L_0} \approx$ 10–20 m), where the relative bias between XBNH and XBSB is 46%. The underestimation is smaller (relative bias of 26%) for more energetic conditions ($\sqrt{H_0 L_0} \gtrapprox 20$ m). However, an underestimation is present for all observed conditions, including those that would be defined as a dissipative beach state according to Wright and Short (1984, ; 16% of the simulations). This indicates that despite recent improvements made to the wave transformation module in XBSB (Roelvink et al., 2017), further investigation of infragravity-band swash processes in XBSB is required.

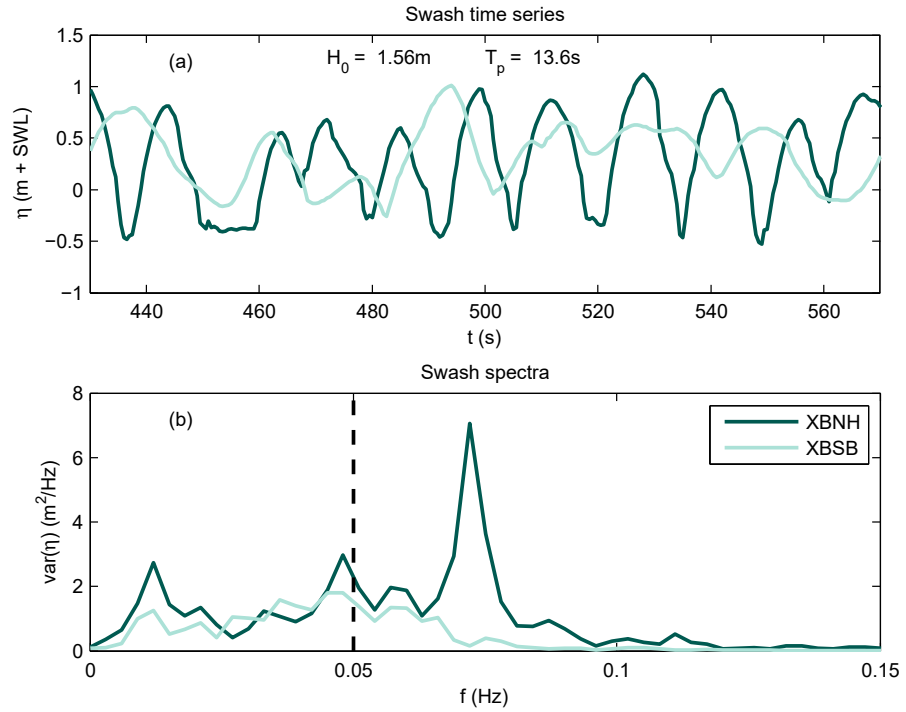

Fig. 7. Example of swash time series (a) and swash spectra (b) in the XBNH and XBSB models for offshore wave conditions of $H_{m0} = 1.57$ m and $T_p = 10.7$ s. Note that in (a) the two models are forced with identical spectral boundary conditions, but individual time series differ because of the use of a random phase model to generate offshore wave boundary conditions. The frequency divide between incident band and infragravity band is marked by a dashed line in (b).

Table 3
Slope of the linear regression lines (see Fig. 8) of the runup components $\overline{\eta}$, S_{inc} and S_{ig} predicted by XBNH and XBSB as function of the relations found by Stockdon et al. (2006). The slopes found by Stockdon et al. (2006) are also included.

Model	Slope (−)		
	$\overline{\eta}$	S_{inc}	S_{ig}
XBNH	0.26	0.68	0.06
XBSB	0.28	0.28	0.04
S2006	0.35	0.75	0.06

4.2. Sources of swash differences between XBSB and XBNH

Improvement in the prediction of S_{inc} using XBNH relative to XBSB is expected given that XBSB does not explicitly resolve incident-band wave motions (cf. Fig. 4). However, as both models resolve infragravity waves, it is expected that predictions of infragravity-band swash motions would be comparable. Observed differences in infragravity-band swash between the XBNH and XBSB models may originate either from outside the swash zone, e.g., due to differences in the incoming infragravity wave field entering the swash zone, as has particularly been shown to occur under wide directional wave spreading by Roelvink et al. (2017), or from within the swash zone, e.g, resulting from explicit simulation of incident-band swash-swash interaction in the swash zone in the XBNH model, leading to the generation of low-frequency motions in the swash (Brocchini and Baldock, 2008), which are not present in the XBSB model.

To differentiate between sources inside and outside the swash zone, one-dimensional (1D) XBNH and XBSB cross-shore profile models of the swash zone for the 50 simulations described in Sections 2.2 and 4.1 were developed. The seaward edge of the swash zone is defined as the most

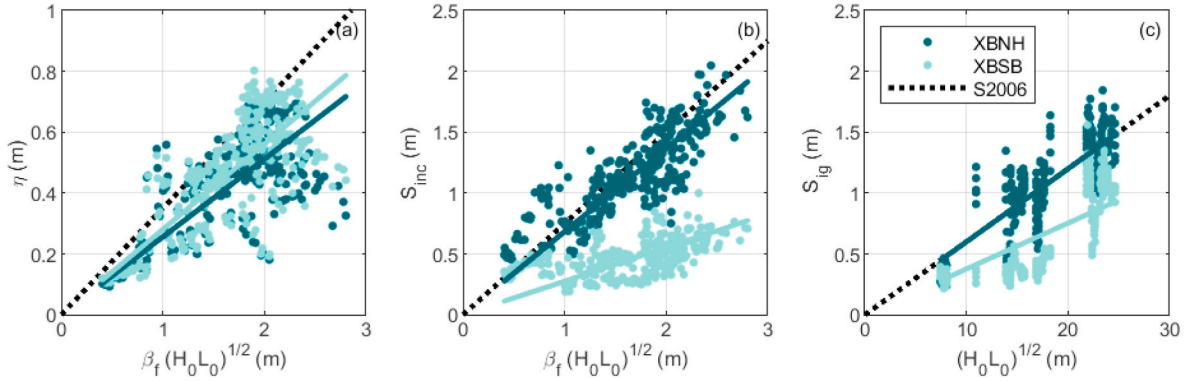

Fig. 8. Setup $\overline{\eta}$, significant incident swash S_{inc} and significant infragravity swash S_{ig} predicted by XBNH and XBSB as a function of the relations found by Stockdon et al. (2006). Linear regression lines have been drawn through the results. The dashed black line indicates these relations including the constant found by Stockdon et al. (2006).

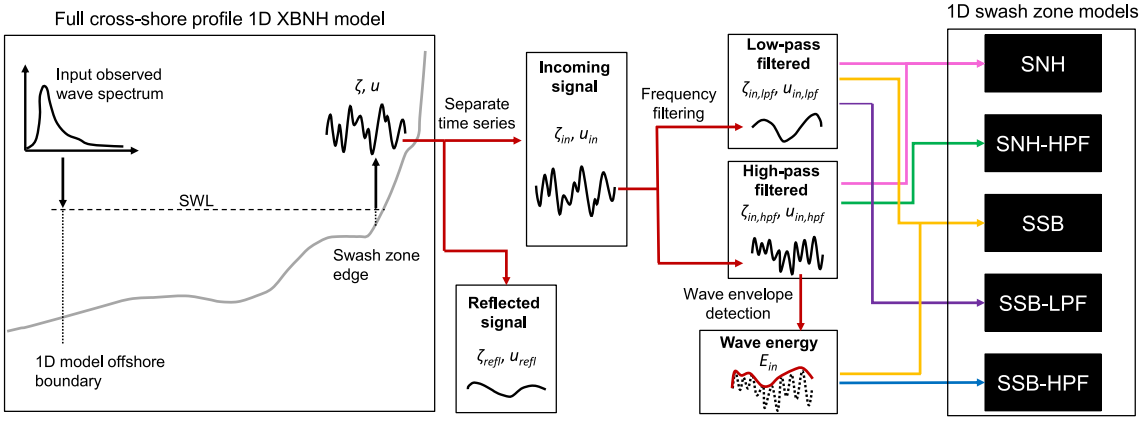

Fig. 9. Schematic of swash zone model boundary conditions.

landward point submerged by at least 0.05 m throughout the simulation period. To generate boundary conditions for the 1D swash-zone models, a 1D XBNH cross-shore transect model was set up using the central cross-shore profile from the 2DH models, and forced by the 50 offshore boundary conditions described in Section 2.2 (see Fig. 9). Time series of surface elevation and cross-shore velocity at the edge of the swash zone in the 1D cross-shore transect model were subsequently separated into incoming and reflected waves following Guza et al. (1984), and the computed incoming wave time series for all 50 simulations were used to derive boundary conditions for the 1D swash zone models.

Five types of swash zone models were run for each of the 50 offshore wave conditions (250 simulations in total; Fig. 9). In SNH, both the incoming incident-band (high-pass filter; $f > 0.05$ Hz) and infragravity-band (low-pass filter; $f \leq 0.05$ Hz) wave signal time series were imposed at the swash-zone boundary of an XBNH model. In SSB, an XBSB model was used to resolve swash-zone hydrodynamics. Flow boundary conditions were generated from the low-pass filtered incoming wave signal time series of the 1D XBNH cross-shore transect model. In addition, time

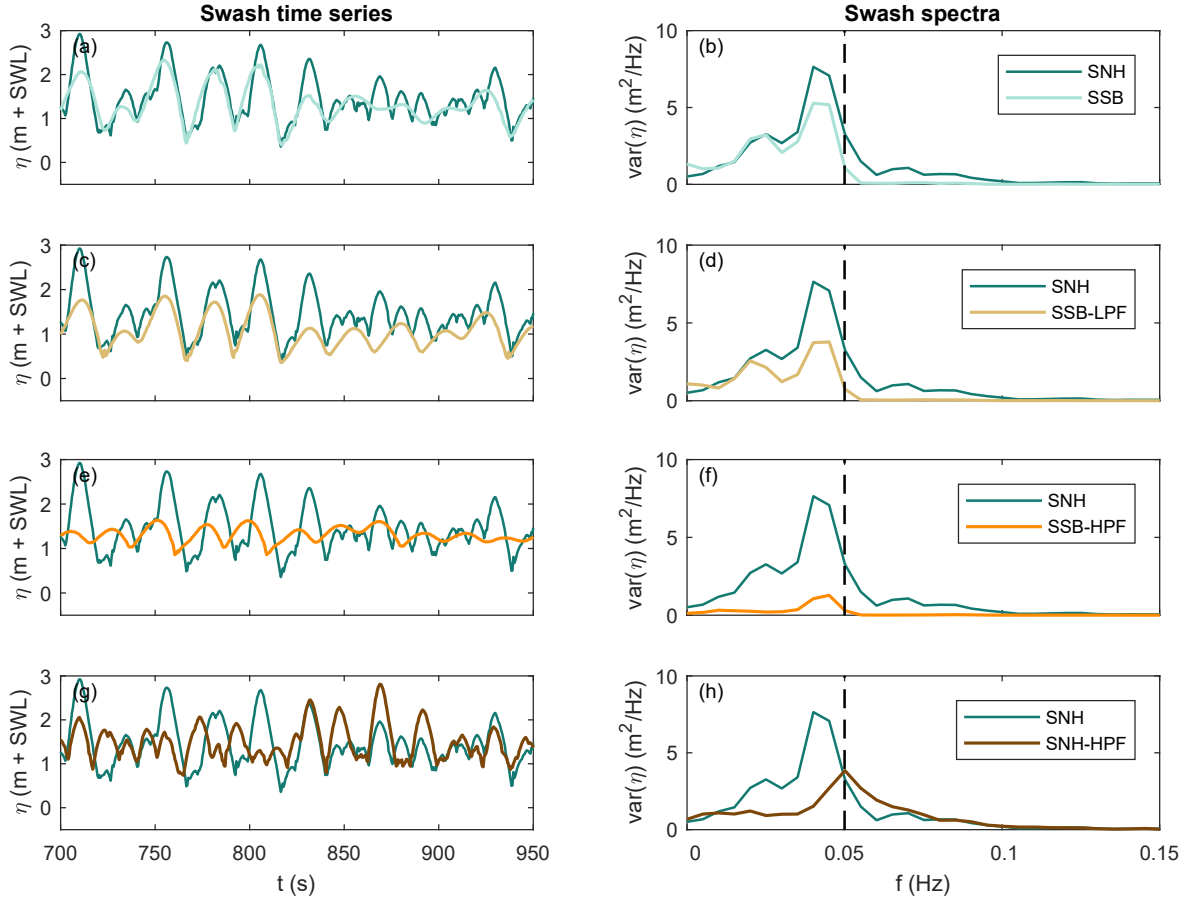

Fig. 10. Time series (left column) and spectra (right column) of swash motions in the SSB (a,b), SSB-LPF (c,d), SSB-HPF (e,f) and SNH-HPF (g,h) swash models relative to those of the SNH swash model for an example simulation with offshore $H_{m0} = 1.44$ m and $T_p = 10.8$ s. The frequency divide between incident band and infragravity band is marked by a dashed line in (b, d, f and h).

series of high-frequency wave energy, varying at the wave-group time scale and derived from the envelope of the incoming high-pass filtered time series (cf. de Vries et al., 2006), were imposed as boundary conditions. It is important to note that while SNH represents a 1D swash-zone equivalent of the 2DH XBNH models described in Section 2.2, SSB is not an analogous swash-zone equivalent of the 2DH XBSB models of Section 4.1, in that the boundary condition forcing for SSB is provided by the 1D XBNH cross-shore transect model, not an XBSB model. Therefore, since their boundary conditions are derived from the same source, differences in swash dynamics between SNH and SSB are solely due to the manner in which incident-band waves are resolved by XBNH and XBSB within the swash zone.

Three additional swash zone models were run in which the imposed boundary conditions contain only low-pass, or high-pass filtered information, to exclude incident-band, or infragravity-band waves at the boundary, respectively. SSB-LPF and SSB-HPF are variants of SSB, in which the incoming incident-band (SSB-LPF) and infragravity-band (SSB-HPF) boundary conditions were selectively removed. SNH-HPF is a variant of SNH that is forced using only incoming incident-band wave motions, without imposing any infragravity-band waves at the swash-zone boundary. Note that since an XBNH swash-zone model with only infragravity-band boundary conditions (i.e., SNH-LPF) provides identical results to SSB-LPF, this swash-zone model type is not included separately in the following analysis.

Relative differences in S_{ig} simulated by the five swash-zone models are quantified for each of the 50 offshore wave condition simulations as:

$$\Delta S^{m}_{ig,rel} = \frac{S^{m}_{ig} - S^{ref}_{ig}}{S^{ref}_{ig}} \tag{6}$$

where the superscript m refers to the swash zone model of interest (i.e., SSB, SSB-LPF, SSB-HPF, or SNH-HPF) and the superscript *ref* refers to the reference swash zone model, in this case SNH (see Fig. 10 for example swash time series and spectra).

The results of the swash zone model analysis are summarized in Fig. 11. The relative difference in S_{ig} between SNH and SSB is small, with a mean underestimation of 5%. This relative difference is significantly smaller than that found for the 2DH XBNH and XBSB models (~33%; cf. Table 3), indicating that the majority (~85%) of the observed difference in S_{ig} found in Section 4.1 is due to differences between the models occurring outside the swash zone. Although further research is required, the more complete description of the incident-band wave spectrum, wave groupiness, and non-linear energy transfers in the shoaling and surf zone in XBNH than in XBSB are likely causes of these differences at the outer edge of the swash zone. The remaining ~15% of the observed difference in S_{ig} must conversely be due to differences occurring inside the swash zone.

The SSB-LPF and SSB-HPF simulations were used to determine if the presence of incident-band wave energy outside of the swash zone contributes to the simulated magnitude of infragravity-band swash. Results from SSB-LPF, which is forced without incident-band wave information, show a greater underestimation of the infragravity-band swash (mean underestimation 15%, see Fig. 11) than SSB. The SSB-HPF simulations, which were forced without incoming infragravity-band waves at the swash-zone boundary, predict non-zero values of S_{ig} (mean underestimation 74%). Both these results show that the presence of incident-band wave energy, which in XBSB varies at the wave-group time scale, at the edge of the swash zone contributes to the generation of infragravity-band swash. Therefore, alongside differences in the incoming infragravity-band energy, differences in incident-band wave energy and groupiness at the edge of the swash zone between XBNH and XBSB may be expected to contribute to simulated differences in S_{ig}.

To examine differences in S_{ig} occurring within the swash zone, the results of SNH-HPF are compared to those of SSB-HPF. In this, SNH-HPF is forced without incoming infragravity-band waves, but with a time series of incoming incident-band waves that are fully resolved in the model. Importantly, SNH-HPF is forced with the same low-frequency wave-group variation of incident-band wave energy as SSB-HPF. SSB-HPF underestimates S_{ig} more than SNH-HPF (74% versus 44% mean underestimation) indicating that the presence of incident-band wave motions within the modelled swash zone leads to increased values of S_{ig}. Cursory analysis shows that given the offshore forcing conditions and beach slope used in the simulations, the swash period (as defined by Brocchini and Baldock, 2008) is such that swash-swash interactions may be expected in approximately half of the 50 simulations, and may therefore cause increased low-frequency variance in SNH-HPF relative to SSB-HPF. However, other sources of low-frequency variance, e.g., low-frequency variance at the wave-group time scale due to increased total swash amplitude, as well as differences in incident-band wave transformation within the swash zone in the SNH-HPF model compared to the SSB-HPF model, may also contribute. For the purpose of this study however, it is sufficient to conclude that differences in simulated values of S_{ig} can occur solely due to the manner in which incident-band waves are resolved within the swash zone.

4.3. Implications for the application of XBSB

The results of Section 3 show that XBNH is generally more accurate in the prediction of swash than the S2006 parameterization, and therefore may be a useful engineering tool for application on intermediate-reflective beaches. In line with Stockdon et al. (2014) however, Section 4.1 shows that the more commonly-used XBSB model typically underestimates wave runup during SD97. Given the more prevalent use of XBSB relative to XBNH in engineering applications, it is relevant to identify under what types of conditions large differences

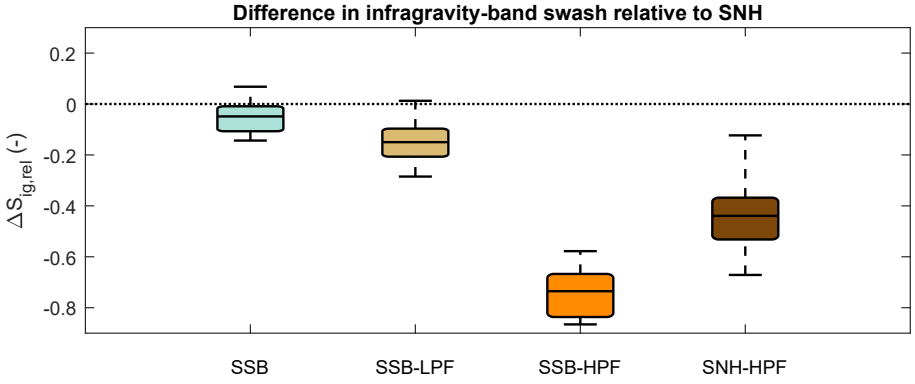

Fig. 11. Box and whisker plots showing difference in infragravity-band significant swash for four swash zone models relative to those of SNH. Spreading is the result of variations in the 50 simulations with varying offshore wave conditions. Box plots indicate the first and third quantile of the data, whiskers the 9% and 91% exceedence values, and the solid line the mean of the data.

between the models occur, and hence for what conditions XBSB may not be suitable to assess wave runup. To this end, 140 additional XBNH and XBSB simulations were set up with a broad range of wave forcing (H_{m0} = 0.6–4.0 m; T_p = 6.0–13.5 s; shore-normal waves with directional spread varying between 10° and 30°). All simulations were carried out using the observed bathymetry of SD97 (17 October), constant offshore water level (NGVD+0.5 m; approximately MSL), and model grid and parameter settings described in the previous sections. The new simulations represent conditions in the range of ω = 1.4–11.2, with ω the dimensionless fall velocity defined as (Dean, 1973; Wright and Short, 1984):

$$\omega = \frac{H_b}{w_s T_p} \tag{7}$$

where H_b is the breaker wave height, w_s the sediment fall velocity and T_p the peak wave period. The breaker wave height is derived following Komar and Gaughan (1972) from the significant wave height and peak period observed at the FRF-8m array, and the fall velocity w_s is computed following Van Rijn (1993) assuming a median grain size of 0.5 mm (Stauble and Cialone, 1996). ω-values smaller than 1 indicate a reflective beach state, ω-values between 1 and 6 correspond to an intermediate beach state, and values larger than 6 to a dissipative beach state.

Differences in model prediction of η, S_{inc}, S_{ig} and $R_{2\%}$ are computed at the location of the six runup transects for the 50 SD97 simulations and the additional 140 simulations as $\Delta X = X_{\mathrm{XBNH}} - X_{\mathrm{XBSB}}$, where the variable X represents any of η, S_{inc}, S_{ig}, or $R_{2\%}$. To account for variations in swash magnitude due to wave forcing, differences are normalized by the deep water wave height H_0 and presented in Fig. 12 relative to ω. The mean normalized difference (or normalized bias) and the root mean square of the normalized difference (normalized RMSD) for different ω-ranges are summarized in Table 4. The results show that the normalized bias in predicted η (panel a) remains relatively constant and small (~2% greater mean setup in XBSB) across the range of wave conditions simulated in this study. As may be expected, the normalized bias in S_{inc} (panel b) is substantially larger for reflective conditions ($\omega \leq 1$) than for dissipative conditions ($\omega > 6$), with a normalized bias of 105% and 20% of the deep water wave height, respectively. Large differences mainly occur for conditions in which the total runup ($R_{2\%}$) as predicted by XBNH is small. In line with the results of Section 4.1, the normalized bias in S_{ig} between XBNH and XBSB (panel c) remains present for all wave conditions simulated in this study. In approximately 15% of the simulations, which are primarily intermediate and reflective wave conditions (28 out of 29 cases), XBSB provides higher predictions of S_{ig} than XBNH. The normalized bias in S_{ig} is therefore relatively low (−2%) for the reflective conditions assessed in this study. However, the normalized RMSD for reflective and intermediate conditions is 15% and 19%, respectively, which is similar to that for dissipative conditions (17%). During dissipative wave conditions, XBSB primarily (65 out of 66 cases) predicts lower infragravity-band swash than XBNH, with a normalized bias of 16%. As the normalized RMSD in η and S_{ig} remains relatively constant across the range of wave conditions assessed in this study, the variation in observed differences in $R_{2\%}$ (panel d) can primarily be attributed to the prediction of S_{inc}. Consequently, the normalized bias in $R_{2\%}$ is large for reflective conditions (57% of the deep water wave height). However, due to the observed difference in S_{ig}, XBSB also predicts lower $R_{2\%}$ for intermediate and dissipative conditions: 18% and 17% of the deep water wave height, respectively.

In line with the findings of Section 4.1, this study shows that, relative to XBNH, XBSB underestimates S_{inc} for all wave conditions and S_{ig} for most intermediate and dissipative wave conditions at the Duck field site. While it is generally well established that XBSB is unable to accurately predict wave runup on reflective beaches (e.g., Roelvink et al., 2017), these results suggest that XBSB may also structurally underestimate wave runup on other dissipative beaches, although to a lesser degree than on reflective beaches. While this potential underprediction appears not to have negatively affected the ability of the model to predict storm-driven morphodynamics under dissipative conditions in other studies (e.g., McCall et al., 2010; Lindemer et al., 2010; de Vet et al.,

Table 4
Normalized bias and normalized RMSD between XBNH and XBSB predictions of $\overline{\eta}$, S_{inc}, S_{ig} and $R_{2\%}$ for different ω-ranges.

	Normalized bias/Normalized RMSD (−)			
ω (−)	$\overline{\eta}$	S_{inc}	S_{ig}	$R_{2\%}$
0–1	0.03/0.07	1.05/1.16	−0.02/0.15	0.57/0.67
1–6	−0.03/0.04	0.33/0.41	0.09/0.19	0.18/0.25
>6	−0.01/0.02	0.20/0.21	0.16/0.17	0.17/0.19
Overall	−0.02/0.04	0.29/0.37	0.11/0.18	0.18/0.24

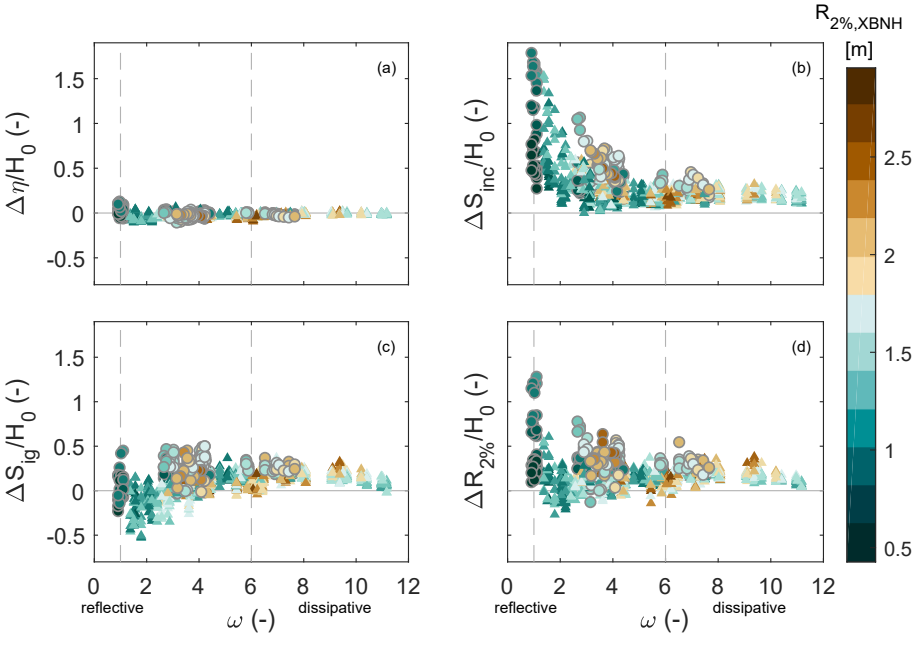

Fig. 12. Normalized difference in η (a), S_{inc} (b), S_{ig} (c) and $R_{2\%}$ (d) between XBNH and XBSB for a range of reflective–dissipative wave conditions. Marker shapes differentiate the original 50 SD97 (○) and 140 additional (△) simulations, whereas marker colours indicate the $R_{2\%}$ value computed by XBNH for every wave condition. Vertical lines distinguish between reflective ($\omega \leq 1$), intermediate ($1 < \omega \leq 6$) and dissipative ($\omega > 6$) conditions. (For interpretation of the references to colour in this figure legend, the reader is referred to the Web version of this article.)

2015; Harter and Figlus, 2017; Passeri et al., 2018; van der Lugt et al., 2019; van Ormondt et al., 2020), the difference between the XBNH and XBSB models is relevant and will affect the assessment of storm-driven high water marks, as well as potentially the prediction of overtopping and overwash volumes. Further assessment of XBSB skill in the prediction of swash and runup relative to observations on more dissipative field sites is therefore greatly recommended to better quantify the true model error of XBSB.

5. Conclusion

Validation of wave runup predicted by numerical models such as XBeach is required to make accurate estimates of the impacts of storms. Here we present the use of the incident-band wave-resolving, non-hydrostatic XBeach model to simulate runup on an intermediate–reflective beach observed during the SandyDuck '97 field experiment. It is shown that wave height is predicted by the model with root mean square errors of 0.17 m and 0.08 m for incident-band and infragravity-band wave height, respectively. The model subsequently simulates swash dynamics and runup on the beach, in which setup at the waterline is slightly underestimated (bias of −0.04 m) with a root mean square error of 0.13 m. Both the incident-band and infragravity-band swash are well represented with low bias (0.06 m and −0.09 m, respectively) and root mean square errors of 0.25 m and 0.23 m. In a quantitative sense, the performance of the XBeach non-hydrostatic model for runup is generally found to be better than that of the commonly-used empirical wave runup model of Stockdon et al. (2006), which itself was derived using data from the SandyDuck '97 field experiment, highlighting the value of the model as a practical tool for estimating wave runup.

The performance of the XBeach non-hydrostatic model was compared to that of the short-wave phase-averaged XBeach surf-beat model. The results show that XBeach surf-beat predicts wave transformation and setup at the waterline similarly to the non-hydrostatic model, but that the XBeach non-hydrostatic model is a better predictor of swash. In line with expectations given the intermediate–reflective nature of the SandyDuck '97 beach, the XBeach surf-beat model underpredicts the observed incident-band swash motions, as well as those simulated in the non-hydrostatic model. Analysis also shows that XBeach surf-beat underpredicts infragravity-band swash observed during the SandyDuck '97 experiment, as well as that simulated in the non-hydrostatic model. Model differences in infragravity-band swash are primarily (~85%) due to differences in the simulated incoming infragravity waves and incident-band wave-group energy occurring offshore of the swash zone, where differences in non-linear energy transfers in the surf zone may play an important role. Model differences in infragravity-band swash are secondarily (~15%) due to the manner in which incident-band waves are resolved within the swash zone.

Exploring a wide range of wave conditions, larger than present during the SandyDuck'97 experiment, and representing a range of reflective to dissipative beach states, it is shown that the XBeach surf-beat model predicts setup at the waterline similarly to the non-hydrostatic model for all conditions. Incident-band swash motions in the XBeach surf-beat model are smaller than those in the non-hydrostatic model for all conditions, in particular for reflective conditions for which differences in the incident-band swash are approximately proportional to the deep water wave height. Infragravity-band swash motions in the surf-beat model are also smaller than those in the non-hydrostatic model, including for dissipative wave conditions where the mean difference between the models is 16% of the deep water wave height. The result of these swash differences is that the surf-beat model underpredicts wave runup relative to the non-hydrostatic model during reflective, and to a lesser extent during dissipative, conditions (normalized differences 57% and 17%, respectively). Further quantification of the difference in infragravity-band waves and swash, including comparison to observations, for more dissipative field sites is highly recommended.

CRediT authorship contribution statement

A.F. de Beer: Conceptualization, Methodology, Software, Formal analysis, Writing - original draft, Visualization. **R.T. McCall:** Conceptualization, Methodology, Software, Formal analysis, Writing - original draft, Writing - review & editing, Visualization, Supervision. **J.W. Long:** Methodology, Resources, Writing - review & editing, Funding acquisition. **M.F.S. Tissier:** Methodology, Writing - review & editing. **A.J.H.M. Reniers:** Methodology, Writing - review & editing.

Declaration of competing interest

The authors declare that they have no known competing financial interests or personal relationships that could have appeared to influence the work reported in this paper.

Acknowledgements

This material is based upon work supported by the U.S. Geological Survey under Grant/Cooperative Agreement No. G14AC00396 and the Deltares Strategic Research Program "Hydro and morphodynamics during extreme events" (12300604). This work benefited from discussions with Ap van Dongeren, who helped define the scope, and Dave Thompson, who supplied us with all the necessary information about the research conducted earlier at USGS. We would like to thank the FRF for the SD97 data and their long-term investment in coastal research. Any use of trade, firm, or product names is for descriptive purposes only and does not imply endorsement by the U.S. government.

References

Brocchini, M., Baldock, T.E., 2008. Recent advances in modeling swash zone dynamics: influence of surf-swash interaction on nearshore hydrodynamics and morphodynamics. Rev. Geophys. 46, 1–21.

Cohn, N., Ruggiero, P., 2016. The influence of seasonal to interannual nearshore profile variability on extreme water levels: modeling wave runup on dissipative beaches. Coast. Eng. 115, 79–92.

Dean, R.G., 1973. Heuristic models of sand transport in the surf zone. In: First Australian Conference on Coastal Engineering, 1973: Engineering Dynamics of the Coastal Zone. Institution of Engineers, Australia, 215.

Guza, R.T., Thornton, E.B., 1982. Swash oscillations on a natural beach. J. Geophys. Res. 87, 483.

Guza, R., Thornton, E., Holman, R., 1984. Swash on steep and shallow beaches. Coastal Engineering Proceedings 1, 708–723.

Harter, C., Figlus, J., 2017. Numerical modeling of the morphodynamic response of a low-lying barrier island beach and foredune system inundated during hurricane ike using xbeach and cshore. Coast. Eng. 120, 64–74.

Klaver, S., Nederhoff, C.M., Giardino, A., Tissier, M.F.S., van Dongeren, A.R., van der Spek, A.J.F., 2019. Impact of coral reef mining pits on nearshore hydrodynamics and wave runup during extreme wave events. J. Geophys. Res.: Oceans 124, 2824–2841.

Komar, P.D., Gaughan, M.K., 1972. Airy wave theory and breaker height prediction. Coast. Eng. 405–418, 1972.

Lashley, C., Roelvink, D., van Dongeren, A., Buckley, M., Lowe, R., 2018. Nonhydrostatic and surfbeat model predictions of extreme wave run-up in fringing reef environments. Coast. Eng. 137, 11–27.

Lindemer, C., Plant, N., Puleo, J., Thompson, D., Wamsley, T., 2010. Numerical simulation of a low-lying barrier island's morphological response to hurricane katrina. Coast. Eng. 57, 985–995.

Longuet-Higgins, M., Stewart, R., 1964. Radiation stresses in water waves; a physical discussion, with applications. Deep Sea Res. Oceanogr. Abstr. 11, 529–562.

van der Lugt, M.A., Quataert, E., van Dongeren, A., van Ormondt, M., Sherwood, C.R., 2019. Morphodynamic modeling of the response of two barrier islands to atlantic hurricane forcing. Estuar. Coast Shelf Sci. 229, 106404.

Matias, A., Masselink, G., Castelle, B., Blenkinsopp, C.E., Kroon, A., 2016. Measurements of morphodynamic and hydrodynamic overwash processes in a large-scale wave flume. Coast. Eng. 113, 33–46. Barrier Dynamics Experiment II: sediment processes across a large-scale sand barrier.

McCall, R., Van Thiel de Vries, J.S.M., Plant, N., Van Dongeren, A.R., Roelvink, J.A., Thompson, D., Reniers, A., 2010. Two-dimensional time dependent hurricane overwash and erosion modeling at Santa Rosa Island. Coast. Eng. 57, 668–683. https://doi.org/10.1016/j.coastaleng.2010.02.006.

McCall, R.T., Masselink, G., Poate, T.G., Roelvink, J.A., Almeida, L.P., Davidson, M., Russell, P.E., 2014. Modelling storm hydrodynamics on gravel beaches with XBeach-G. Coast. Eng. 91, 231–250.

Van der Meer, J.W., Stam, C.M., 1992. Wave Runup on Smooth and Rock Slops of Coastal Structures.
Neumann, B., Vafeidis, A.T., Zimmermann, J., Nicholls, R.J., 2015. Future coastal population growth and exposure to sea-level rise and coastal flooding - a global assessment. PLOS ONE 10, 1–34.
Nicolae Lerma, A., Pedreros, R., Robinet, A., Sénéchal, N., 2017. Simulating wave setup and runup during storm conditions on a complex barred beach. Coast. Eng. 123, 29–41.
van Ormondt, M., Nelson, T.R., Hapke, C.J., Roelvink, D., 2020. Morphodynamic modelling of the wilderness breach, fire island, New York. part i: model set-up and validation. Coast. Eng. 157, 103621.
Palmsten, M.L., Splinter, K.D., 2016. Observations and simulations of wave runup during a laboratory dune erosion experiment. Coast. Eng. 115, 58–66.
Passeri, D.L., Long, J.W., Plant, N.G., Bilskie, M.V., Hagen, S.C., 2018. The influence of bed friction variability due to land cover on storm-driven barrier island morphodynamics. Coast. Eng. 132, 82–94.
Pearson, S.G., Storlazzi, C.D., van Dongeren, A.R., Tissier, M.F.S., Reniers, A.J.H.M., 2017. A bayesian-based system to assess wave-driven flooding hazards on coral reef-lined coasts. J. Geophys. Res.: Oceans 122, 10099–10117.
Poate, T.G., McCall, R.T., Masselink, G., 2016. A new parameterisation for runup on gravel beaches. Coast. Eng. 117, 176–190.
Reniers, A., MacMahan, J., Thornton, E., Stanton, T., 2006. Modelling infragravity motions on a rip-channel beach. Coast. Eng. 53, 209–222.
Van Rijn, L.C., 1993. Principles of Sediment Transport in Rivers, Estuaries and Coastal Seas, 1006. Aqua publications, Amsterdam.
Rijnsdorp, D.P., Ruessink, G., Zijlema, M., 2015. Infragravity wave dynamics in a barred coastal region, a numerical study. J. Geophys. Res.: Oceans 120, 4068–4089.
Roelvink, D., Reniers, A., van Dongeren, A., van Thiel de Vries, J., McCall, R., Lescinski, J., 2009. Modelling storm impacts on beaches, dunes and barrier islands. Coast. Eng. 56, 1133–1152.
Roelvink, D., van Dongeren, A., McCall, R., Hoonhout, B., van Rooijen, A., van Geer, P., de Vet, L., Nederhoff, K., Quataert, E., 2015. XBeach Technical Reference : Kingsday Release. Technical Report April. Deltares.
Roelvink, D., McCall, R., Mehvar, S., Nederhoff, K., Dastgheib, A., 2017. Improving predictions of swash dynamics in XBeach: the role of groupiness and incident-band runup. Coast. Eng. 1–21.
Ruessink, B.G., Kleinhans, M.G., van den Beukel, P.G.L., 1998. Observations of swash under highly dissipative conditions. J. Geophys. Res. 103, 3111.
Sallenger Jr., A.H., 2000. Storm impact scale for barrier islands. J. Coast Res. 16, 890–895.
Senechal, N., Abadie, S., Gallagher, E., MacMahan, J., Masselink, G., Michallet, H., Reniers, A., Ruessink, G., Russell, P., Sous, D., Turner, I., Ardhuin, F., Bonneton, P., Bujan, S., Capo, S., Certain, R., Pedreros, R., Garlan, T., 2011. The ECORS-Truc Vert'08 nearshore field experiment: presentation of a three-dimensional morphologic system in a macro-tidal environment during consecutive extreme storm conditions. Ocean Dynam. 61, 2073–2098.
Smit, P., Stelling, G., Roelvink, J., Van Thiel de Vries, J., McCall, R., Van Dongeren, A., Zwinkels, C., Jacobs, R., 2010. XBeach: Non-hydrostatic Model: Validation, Verification and Model Description. Delft University of Technology. Technical Report.
Smit, P., Zijlema, M., Stelling, G., 2013. Depth-induced wave breaking in a non-hydrostatic, near-shore wave model. Coast. Eng. 76, 1–16.
Stauble, D.K., Cialone, M.A., 1996. Sediment dynamics and profile interactions: Duck 94. Coast. Eng. 3921–3934, 1996.
Stockdon, H.F., Holman, R.A., Howd, P.A., Sallenger, A.H., 2006. Empirical parameterization of setup, swash, and runup. Coast. Eng. 53, 573–588.
Stockdon, H.F., Thompson, D.M., Plant, N.G., Long, J.W., 2014. Evaluation of wave runup predictions from numerical and parametric models. Coast. Eng. 92, 1–11.
de Vet, P.L.M., McCall, R.T., Den Bieman, J.P., Stive, M.J., Van Ormondt, M., 2015. Modelling dune erosion, overwash and breaching at fire island (ny) during (h) urricane (s)andy. In: The Proceedings of the Coastal Sediments 2015. World Scientific, pp. 1–10.
de Vries, J.V.T., van de Graaff, J., Raubenheimer, B., Reniers, A., Stive, M., 2006. Modeling inner surf hydrodynamics during storm surges. Coast. Eng. 896–908, 2006.
Wright, L., Short, A., 1984. Morphodynamic variability of surf zones and beaches: a synthesis. Mar. Geol. 56, 93–118.
Zijlema, M., Stelling, G., Smit, P., 2011. SWASH: an operational public domain code for simulating wave fields and rapidly varied flows in coastal waters. Coast. Eng. 58, 992–1012.